Article

Electrochemical Properties of Carbon Nanobeads and Mesophase-Pitch-Based Graphite Fibers as Anodes for Rechargeable Lithium-Ion Batteries

Liyong Wang [1][ID], Tiantian Liu [1], Shengsheng Ji [1], Shiwen Yang [1], Huiqi Wang [1],* and Jinhua Yang [2],*

[1] School of Energy and Power Engineering, North University of China, Taiyuan 030001, China; nucc@nuc.edu.cn (L.W.)
[2] National Key Laboratory of Advanced Composites, AECC Beijing Institute of Aeronautical Materials, Beijing 100095, China
* Correspondence: hqiwang@nuc.edu.cn (H.W.); yangjinhua08@163.com (J.Y.)

Abstract: Various strategies have been devised to enhance the specific capacity (over 372 mA h g^{-1}) and the cycle life of pure carbon-based anode materials for lithium-ion batteries (LIBs). Herein, we have prepared carbon nanobeads (CNBs) with inner onion-like carbon layer structures using chemical vapor deposition. Additionally, mesophase-pitch-based graphite fibers (MPGFs) were fabricated via the melt spinning method. MPGFs had a reversible capacity of 328.2 mA h g^{-1} with a steady Coulombic efficiency after 105 cycles (at 0.05 mA g^{-1}). When cycled at 0.2 A g^{-1}, the CNBs kept a reversible capacity of 586.2 mA h g^{-1} after 256 cycles with stable Coulombic efficiency. The onion-like carbon layer structures of CNBs were beneficial to the storage of lithium ions. In this work, CNBs were fabricated with inner onion-like carbon layer structures to enhance the electrochemical performance of LIBs.

Keywords: carbon nanobeads; mesophase-pitch-based graphite fibers; anode materials; lithium-ion batteries

1. Introduction

Compared to the past, with the increasing development of global society, the demand for energy and quality of life have further improved. Facing environmental pollution and fossil resource consumption, renewable energy has been developed and is utilized in industrial production and daily life [1–4]. Hence, energy storage devices have become one of the most important key links. Rechargeable lithium-ion batteries (LIBs) can store and release electric energy for electronic products. During 2019, John B. Goodenough, M. Stanley Whittingham, and Akira Yoshino won the Nobel Prize due to their great contributions to LIBs [5]. In LIBs, artificial graphite was prepared as the anode material for commercial application [6–9]. Many factories produce graphite for LIBs in the market. In previous research, carbon-based materials were prepared and used for LIBs. They can be classified as one-dimensional carbon nanotubes (CNTs) [10–12], two-dimensional graphene [13–16], and graphite [17–21]. Meanwhile, other materials have also been studied as anode materials for LIBs [22–25]. Silicon possesses a superhigh capacity of 4200 mA h g^{-1}. It has been considered a potential anode for LIBs [26–28]. However, it undergoes structure and volume changes with a 400% volume expansion during alloying and conversion reactions. Zhu et al. fabricated a nano-porous silicon network with controllable porosity and thickness. Its first discharge capacity was 2570 mA h g^{-1}, and its corresponding current rate was at C/10. After 20 cycles, the discharge capacity was kept at 1800 mA h g^{-1}. The porous structure effectively reduced the attenuation of energy storage performance in the silicon anode. When tested at a 1 C current rate, its capacity dropped to 1200 mA h g^{-1} after 200 charge–discharge cycles [29]. Yi cui et al. designed the core–shell structure for silicon-anode materials to obtain high capacity and good Coulombic efficiency [30]. They showed a

way to encapsulate silicon microparticles via conformally synthesized cages of multilayered graphene. The prepared graphene cages permitted silicon to expand and shrink during the cycles in order to obtain a high capacity. The graphene cage also formed a stable solid electrolyte interface (SEI) to increase Coulombic efficiency in the early process. At the C/2 current rate, silicon with a graphene cage was kept over 1200 mA h g^{-1} after 400 cycles. The above method restrained the fracture of silicon microparticles and stabilized SEI during the long cycle life.

Germanium is also a new candidate for carbon-based anode material in LIBs [31–33]. It has a theoretical capacity of over 1624 mA h g^{-1}. A two-step method was presented to fabricate the binder-free germanium anode [34]. The two-step realization process contained a plasma-enhanced chemical vapor deposition (CVD) to grow a germanium film. Then, they were treated using hydrofluoric acid electrochemical etching. The germanium anode kept a 95% capacity retention after a long cycle life (at 1 C current rate, 600 cycles, RT). In particular, it could obtain a 1060, 450 mA h g^{-1} at 10 C and 60 C current rates, respectively. Though the capacity of non-carbon-based anode material is higher than that of ideal graphite, carbon materials have an absolute advantage, considering technical and safety factors in the production process.

Carbon nanotubes have good thermal and electrical conductivity, which is beneficial to enhance the electrical conductivity of the electrode. However, the carbon nanotube needs to combine other assistant materials to obtain a high specific capacity. Using a template synthesis, a three-dimensional architecture composed of one-dimensional graphitized carbon nanotubes and coated with the nitrogen and oxygen elements was prepared [35]. Due to this one-dimensional path, lithium ions can diffuse fast in the intercalation/extraction process. As a freestanding anode for LIBs, it obtained a high capacity of 624 mA h g^{-1} at a rate of 100 mA g^{-1}. Similarly, boron-doped carbon nanotubes were prepared as anode material for LIBs [36]. The electrode delivered a high capacity of 169 mA h g^{-1} at 10 A g^{-1} with excellent long-term stability (5000 cycles). Because of its one-dimensional nanostructure, the carbon nanotube has a lower capacity compared with that of graphene. The ideal graphene's capacity is 837 mA h g^{-1} in theory [37]. It has unique thermal and electrical conductivity, which can also be applied in different fields, such as energy storage, composite materials, and the catalysis industry [38,39]. Porous graphene was synthesized via the CVD method [40]. Porous graphene had a pore size of 3–8 nm with a lot of edges. Its initial reversible capacity was 1827 mA h g^{-1} at a 0.1 C current rate. It delivered a capacity of over 800 mA h g^{-1} at a 1 C current rate after 100 cycles. Surprisingly, it kept about 200 mA h g^{-1} at a 20 C current rate after 100 cycles. The porous structure and high specific surface gave rise to a rather high capacity for graphene used as anode materials. Graphene nanobuds were prepared on Cu foil using the CVD method [41]. As an electrode in LIBs, the graphene nanobuds exhibited a high specific capacity of 2813 mA h g^{-1} at a current density of 4 A g^{-1} in the first discharge–charge process. It maintained a stable capacity of 1600 mA h g^{-1} at 8 A g^{-1} for over 330 cycles. It also had a good Coulombic efficiency of 99%. The anode still obtained a capacity of 870 mA h g^{-1} when tested at a higher current density of 40 A g^{-1}. This outstanding electrochemical performance resulted from the loose space and hollow spaces of few-layered graphene.

Carbon materials with an onion-like structure were used as the anode material for LIBs via the one-step laser-etched method [42]. It delivered a capacity of 436 mA h g^{-1} at a current density of 0.05 A g^{-1}. Even at a rather high current rate of 10 A g^{-1}, a capacity of 89 mA h g^{-1} was obtained. Its concentric structure ensured structural integrity for the electrode, facilitating intrinsic cyclic stability during lithium storage. Graphite could be modified using the pulsed laser annealing method, which introduced a defect into graphite in a controlled way [43]. This also increased the density of lithium-ion trapping sites. The capacity was 430 mA h g^{-1} after the laser treatment. The trapping sites enhanced lithium-ion absorption during the charge–discharge process.

Carbon materials can obtain a high capacity over the theoretical capacity of graphite through structural design and regulation in view of the above work. Herein, carbon

nanobeads (CNBs) were prepared via the CVD method using nickel particles as a catalyst and acetylene as a carbon source. CNBs had an onion-like carbon layer structure on its insides. This effectively enhanced the kinetics of ion diffusion, which enhanced the reversible capacity and rate performance of the CNB anode. As anode materials, CNBs maintained the first discharge capacity and charge capacity of 723.7 and 693.6 mA h g^{-1} at 50 mA g^{-1}, respectively. After four cycles, the CNBs obtained a high reversible capacity of 1273 mA h g^{-1}. When cycled at a current density of 0.2 A g^{-1}, CNBs kept a reversible capacity of 586.2 mA h g^{-1} after 256 cycles. The onion-like carbon layer structures of CNBs were beneficial to the storage of lithium ions. This work provides a simple strategy to fabricate CNBs with inner onion-like carbon layer structures to enhance the electrochemical performance of the LIBs.

2. Materials and Methods

2.1. Materials

CNBs were prepared via the CVD method at 873 K. Acetylene was used as a carbon source, and nickel particles were used as catalysts. Mesophase pitch-based graphite fibers (MPGFs) were fabricated through the a melt-spinning method. The pitch's softening point was 553 K. Initially, the pitch was spun into raw fibers. These as-spun fibers were treated at 553 K under an air atmosphere. Subsequently, the fibers were heated at 1273 K under a nitrogen atmosphere. At last, the resulting carbon fibers were ultimately heated at 3073 K, and the atmosphere was argon.

2.2. Method Characterizations and Electrochemical Evaluation

The samples were analyzed via the X-ray diffraction system (XRD; Bruker AXS D8, Karlsruhe, Germany), field-emission scanning electron microscopy (SEM; JSM-7001F, JEOL, Tokyo, Japan), and field-emission transmission electron microscopy (TEM; JEM-2100F, JEOL Tokyo, Japan) for crystalline structure examination morphology observation and microstructure analysis, respectively, along with molecular structure information studies.

Working electrodes were made of active material, acetylene black, and polyvinylidene fluoride (PVDF). Their weight ratio was 8:1:1. CR Li foil was used as the counter electrode and reference electrode in the cells. The separator was a microporous polypropylene film (Celgard 2400). The used electrolyte was composed of 1 M $LiPF_6$ in ethylene carbonate–dimethyl carbonate (1:1 by volume) and 5 vol. % vinylene carbonates. The cells were tested using a battery test system (LAND CT 2001A model, Wuhan Jinnuo Electronics Ltd., Wuhan, China) at room temperature. The electrochemical workstation was applied to study the electrochemical properties of the samples (CHI660E, Shanghai Chenhua Instrument Ltd., Shanghai, China). The specific surface area adsorption instrument was fabricated by Beijing Jingwei Gao Bo Science and Technology Co., Ltd., Beijing, China (BK112T).

3. Results and Discussion

The macroscopic morphology of CNBs is illustrated in Figure 1a. To facilitate a clear observation of their morphology, high-magnification images are presented in Figure 1b–d. A three-dimensional morphology was formed by the random stacking of numerous CNBs, which exhibited an average diameter of approximately 100 nm. Moreover, as shown in Figure 1c,d, CNBs could arrange themselves into quasi-one-dimensional chain structures. In Figure 1e, a selected area scan is displayed to provide further detail. These CNBs were synthesized using the CVD method and possessed a high purity of carbon content with a minimal oxygen content, as demonstrated in Figure 1f. Typically, graphite anode materials for LIBs underwent treatment at temperatures exceeding 2500 K for purification purposes. For convenient comparison and control purposes, mesophase-pitch-based graphite fibers (MPGFs) were prepared, as depicted in Figure 1g. There were a lot of graphite folds in the inner fibers, as depicted in Figure 1h, which is the typical structure of MPGFs. The diameter of MPGFs was approximately 11 μm. Notably, the inner structure of these fibers exhibited

abundant graphite folds, as shown in Figure 1h. This represents a typical characteristic feature of MPGFs.
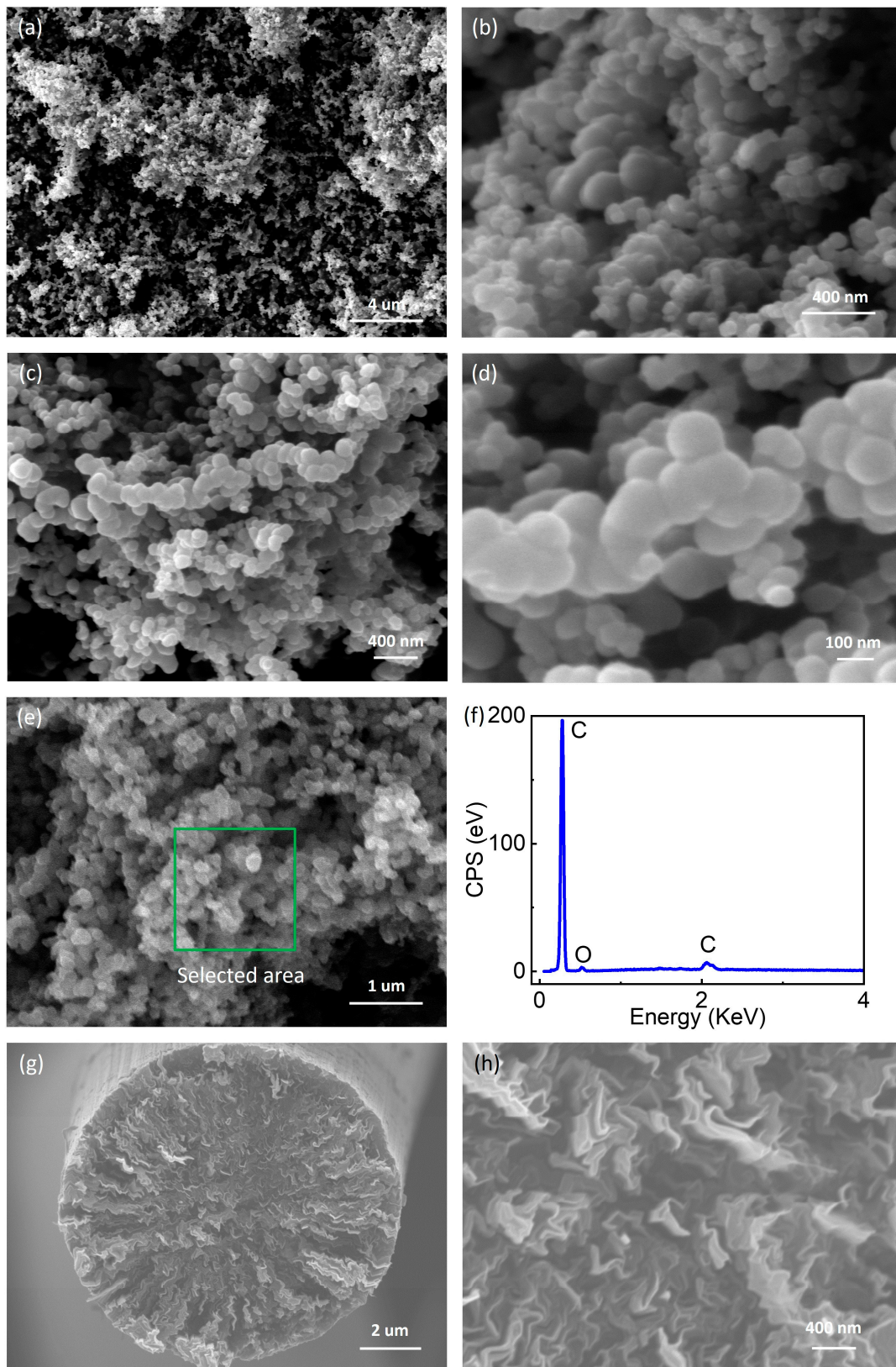
Figure 1. SEM images: (**a–e**) The morphology of CNBs, (**f**) The selected area scanning test of (**e**), (**g**) The cross-section morphology of MPGFs, (**h**) The graphite fold of MPGFs.

The microstructure of the material primarily determines its physical and electrochemical properties. The TEM images of CNBs are shown in Figure 2a,b, revealing quasi-one-dimensional bead chain structures. The electron diffraction pattern exhibited diffraction rings, as depicted in Figure 2c, indicating a disordered structure resulting from low-temperature preparation processes. In Figure 2d, the carbon layer was distinctly visible and arranged circularly, resembling an onion-like structure. Notably, Figure 2e demonstrates evident graphite stripes within MPGFs that were uniformly distributed using a characteristic commonly observed in internationally recognized MPGFs on the market. Furthermore, highly graphitic structures are indicated by highlighted diffraction spots obtained from the entire area, as illustrated in Figure 2f, owing to the presence of graphite grain ribbons within MPGFs, which contributed to their excellent electrical conductivity.
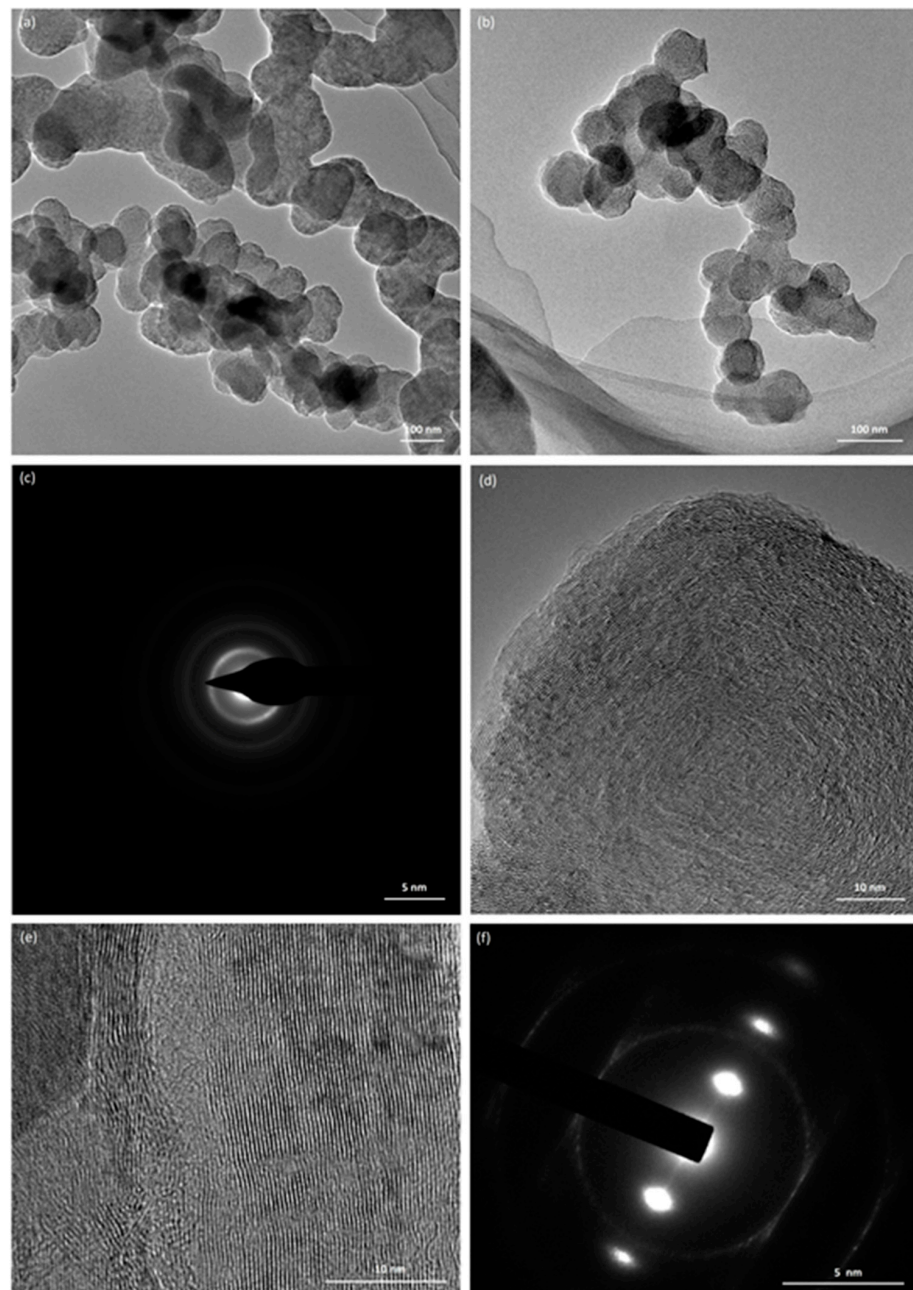
Figure 2. TEM image of CNBs (**a**,**b**,**d**) and MPGFs (**e**), Electron diffraction spots of CNBs (**c**) and MPGFs (**f**).

The structural characteristic of the samples was measured using XRD, as shown in Figure 3. Theoretical interplanar spacing is 0.3354 nm. The interplanar spacing of the CNBs was 0.351 nm. Hence, CNBs had a slightly turbostratic structure. In the case of MPGFs, it was 0.339 nm. MPGFs had a good crystal structure due to graphitization at high temperatures. The above data analysis was consistent with that of TEM.
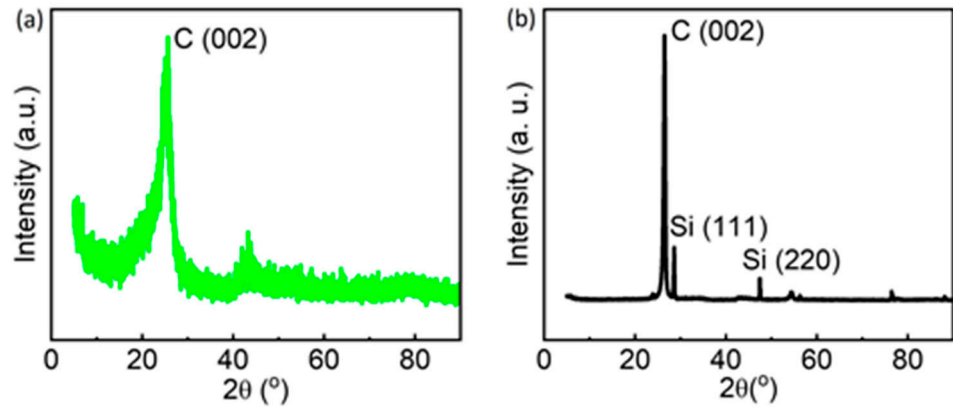

Figure 3. XRD pattern of CNBs (**a**) and MPGFs (**b**).

MPGF were tested at a current density of 50 mA g^{-1}, as depicted in Figure 4a,b. The MPGFs electrode first obtained a charge capacity of 351.25 mA h g^{-1} (Figure 4a). With the increase in the graphitization degree, the structure of graphite material was more stable, and its conductivity was much better. During the whole process, the highest charge capacity was 357.96 mA h g^{-1} at the 70th cycle. It was near the theoretical capacity of ideal graphite. However, it maintained a capacity of 328.2 mA h g^{-1} after 105 cycles.
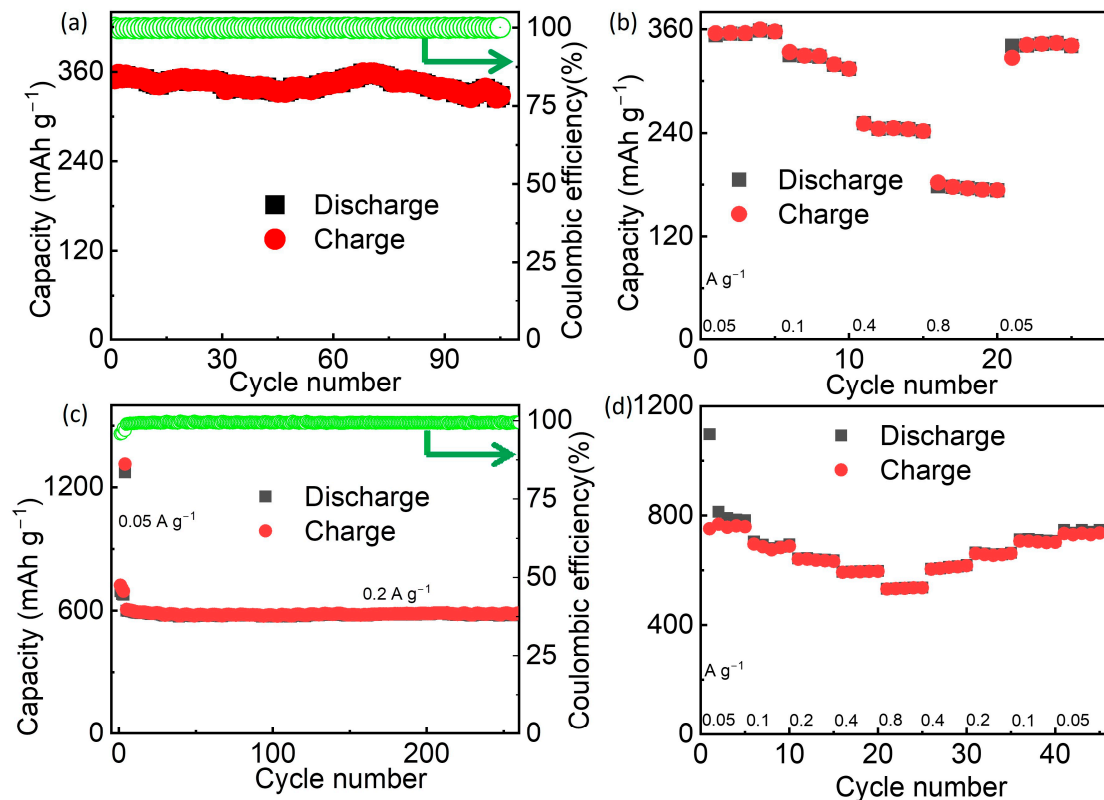

Figure 4. (**a**) Cycle performance of MPGFs, (**b**) Rate capability of MPGFs, (**c**) Cycle performance of CNBs, and (**d**) Rate capability of CNBs.

Rate capability is shown in Figure 4. The current density increased from 50 mA g^{-1} to 800 mA g^{-1} and then switched back to the initial current density. MPGFs delivered the reversible capacity of 350.4, 314.2, 244.5, and 173.5 mA h g^{-1} after 5, 10, 15, and 20 cycles. At last, MPGF electrodes were tested at 50 mA g^{-1} and kept a reversible capacity of 340.5 mA h g^{-1}. The above data show that its rate capability was good, as shown in Figure 4b.

In the case of CNBs, they were cycled at a current density of 50 mA g^{-1}. The CNBs' initial discharge and charge capacity were 723.7 and 693.6 mA h g^{-1}, respectively (Figure 4c). After four cycles, the CNBs obtained a high reversible capacity of 1273 mA h g^{-1}. Then, they were cycled at 0.2 A g^{-1} to examine the cycle performance. At this stage, the initial discharge capacity was 606.2 mA h g^{-1}, and the first charge capacity was 599.7 mA h g^{-1}. In the 256 subsequent cycles, CNBs kept a capacity of 586.2 mA h g^{-1}, which was near the initial charge capacity. During the whole process at the second stage, the whole Coulombic efficiency was very stable with no huge ups and downs. The capacity was more than 572 mA h g^{-1} during the whole process. It mainly came from the disordered microstructure of CNBs. Though the CNBs had a lower graphitization degree, they obtained wider carbon layer spacing for the transport of lithium ions. MPGFs had two-dimensional carbon layer spacing to store the lithium ions. As CNBs, they had a three-dimensional spherical structure with an inner onion-like carbon layer microstructure. An onion-like carbon layer structure in CNBs was beneficial to the storage of lithium ions. This is also one of the reasons why CNBs can have a high lithium-ion storage performance.

During the rate of measurement, as depicted in Figure 4d, the charge capacity of CNBs was 751.9 mA h g^{-1} under a current density of 50 mA g^{-1} after 5 cycles. At the current density of 100, 200, 400, and 800 mA g^{-1}, CNBs obtained a reversible capacity of 688.3, 632.7, 596.3, and 536.2 mA h g^{-1}, respectively. Then, the current density was restored to the previous current density. The corresponding reversible capacity was 617.1, 661.5, 702.4, and 736.5 mA h g^{-1}, respectively. This should be the result of the microstructure of the CNBs, which enhanced the structural integrity and the capacity of the electrode.

In previous research work, carbon nanomaterials were performed in a different capacity as anode material for LIBs. Several anode materials with their performances are listed in Table 1. Porous graphene obtained a capacity of 142 mA h g^{-1} at 2 A g^{-1} after 1200 cycles [44]. The porous structure gave rise to a high capacity for graphene. Hard carbon/graphene composites could obtain 623 mA h g^{-1} at a current density of 0.1 A g^{-1} after 500 cycles [45]. Graphene with a nano-mesh structure maintained a capacity of 1221 mA h g^{-1} at a current density of 0.005 A g^{-1} after 100 cycles [46]. Graphene sheets maintained a capacity of 730 mA h g^{-1} at a current density of 0.0744 A g^{-1} after 200 cycles [47]. Carbon nanofibers kept a capacity of 323 mA h g^{-1} at a current density of 1 A g^{-1} after 1000 cycles [48]. Their three-dimensional structure and good electrical conductivity were beneficial to the capacity. In this work, CNBs obtained a capacity of 596.2 mA h g^{-1} at a current density of 0.2 A g^{-1} after 256 cycles. The CNBs were prepared at low temperatures compared with graphite and had not been graphitized. Hence, CNBs had no ideal graphite structure, graphene sheets, or a graphene nano-mesh structure. They could not have a rather high capacity of over 1200 mA h g^{-1} (graphene nanomeshes anode). But, the CNBs had a disordered carbon layer structure. This helps to improve the performance of lithium storage.

**Table 1.** Application of carbon materials in LIBs.

Number	Anode Material	Current Density (A/g)	Cycle Number	Capacity (mAh g^{-1})	Reference
1	Porous graphene	2	1200	142	[44]
2	Graphitized CNTs	0.1	150	527	[35]
3	Hard-carbon/graphene	0.1	500	623	[45]
4	graphene nanomeshes	0.05	100	1221	[46]
5	Graphene sheets	0.0744	200	730	[47]
6	Graphitic onion-like carbon	1	300	312	[42]
7	Carbon nanofibers	1	1000	323	[48]
8	CNBs	0.2	256	596.2	This work

Carbon atoms usually rearrange during the graphitization process, which usually eliminates some hole structures or defects. Ideal graphite without a pore structure has a theoretical capacity of 372 mAh g^{-1}. But carbon materials usually have an inner-pore structure and defective structure, which can provide a much more specific capacity over 372 mAh g^{-1} [49–51]. CNBs were prepared at a low temperature compared with graphite. Hence, there was a certain pore structure in the inner parts of CNBs. The pore volume–pore distribution diagram is shown in Figure 5. The mean pore size of adsorption was 8.59 nm. This helped to improve the performance of lithium storage.
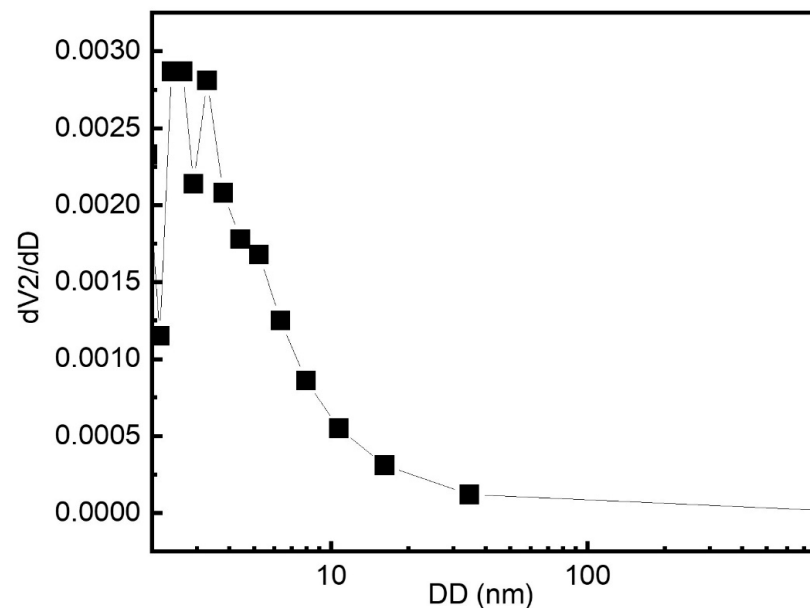
Figure 5. Volume–pore distribution diagram.

A typical cyclic voltammetry (CV) measurement of the samples is shown in Figure 6. Figure 6a shows the CV curves of MPGFs. Its sweep rate of the potential was 1 mV/s. In the first cathodic half-cycle, the discharge current became large at the starting potential of 1.0 V, which resulted in the formation of the SEI film. The first anodic peak appeared at 0.68 V. The anodic peak shifted to 0.63 V, and the cathodic peak was located at 0.12 V in the following process. In addition, the anodic current peaks of the following scan presented a slightly enhanced intensity compared with the first scan. In the case of the CNB electrode, the discharge current increased gradually from 1.41 V, which could be attributed to the formation of an SEI film in the first cycle. This resulted in an initial irreversible capacity, as shown in Figure 6c. The corresponding sweep rate of the potential was 10 mV/s. In the first anodic scan, two obvious anodic peaks appeared at 0.88 and 1.26 V. During the following scan, the corresponding peaks overlapped quite well. Judging from the three curves of CNB electrodes, they overlapped quite well, suggesting their good cycling performance.
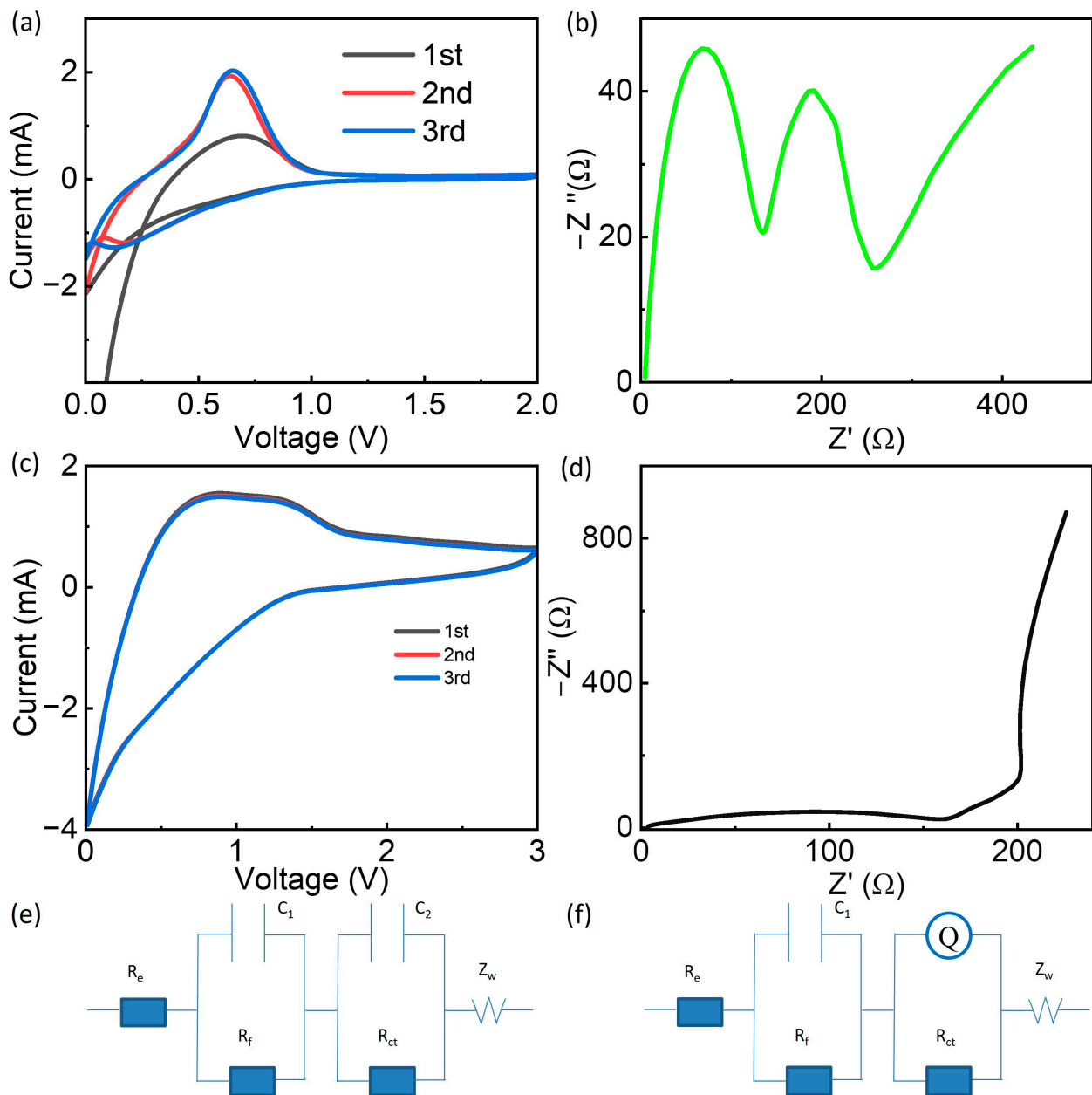
Figure 6. (**a**) Cyclic voltammetry curves, and (**b**) Nyquist plots of MPGFs, (**c**) Cyclic voltammetry curves, and (**d**) Nyquist plots of CNBs, (**e**) Equivalent circuit of MPGFs, and (**f**) Equivalent circuit of CNBs.

The electrolyte resistance is represented by R_e in the equivalent circuit shown in Figure 6e,f, while R_{ct} denotes the charge transfer resistance, and R_f represents the resistance of the surface film and contact. Additionally, Q is the double-layer constant phase angle element, and Z_w is the Warburg impedance in relation to the diffusion of lithium ions into the bulk of the composite electrode. C is the capacitance. The equivalent circuit of MPGFs is as shown in Figure 6e; the R_e was 12 Ω, the R_f was 110 Ω, and the R_{ct} was 119 Ω, respectively. The equivalent circuit of CNBs is depicted in Figure 6f. The corresponding R_e was 21 Ω, and the R_f was 122 Ω. The CNBs had a lower graphitization degree. The lower heat treatment temperature resulted in relatively weak conductivity compared with that of MPGFs. Hence, the R_{ct} of CNBs was higher than that of MPGFs. This was because CNBs were prepared at a low temperature, which resulted in a lower electrical conductivity compared with that of the commercial graphite anode. CNBs also had a larger specific

surface area than that of the MPGFs. Hence, CNBs had a larger impedance than that of the graphite anode.

4. Conclusions

CNBs were prepared with an inner onion-like carbon layer structure using chemical vapor deposition. MPGFs were fabricated via the melt-spinning method. Both kinds of carbon materials were used as anode materials for LIBs. The MPGFs had a reversible capacity of 328.2 mA h g^{-1} with a steady Coulombic efficiency after 105 cycles at a current rate of 0.05 mA g^{-1}. CNBs were graphitized. They had disordered carbon layers and a certain pore structure. Their mean pore size of adsorption was 8.59 nm, which helped to improve the performance of lithium storage. The CNBs kept a reversible capacity of 586.2 mA h g^{-1} after 256 cycles with stable Coulombic efficiency at a current rate of 0.2 A g^{-1}. The onion-like carbon layer structures of CNBs gave rise to the storage of lithium ions. CNBs also had a good rate capability compared with MPCFs. In this work, CNBs with an inner onion-like carbon layer structure were prepared as anode materials to enhance the specific capacity of LIBs.

Author Contributions: L.W.: Conceptualization, validation, writing—original draft preparation, drafting the work, writing—review and editing, funding acquisition. T.L., S.Y. and S.J.: investigation, formal analysis. H.W. and J.Y.: project administration, funding acquisition, conceptualization. All authors have read and agreed to the published version of the manuscript.

Institutional Review Board Statement: Not applicable.

Informed Consent Statement: Not applicable.

Data Availability Statement: Data are contained within the article.

Conflicts of Interest: The authors declare no conflict of interest.

References

1. Koroneos, C.; Spachos, T.; Moussiopoulos, N. Exergy analysis of renewable energy sources. *Renew. Energy* **2003**, *28*, 295–310. [CrossRef]
2. Mahon, H.; O'Connor, D.; Friedrich, D.; Hughes, B. A review of thermal energy storage technologies for seasonal loops. *Energy* **2022**, *239*, 122207. [CrossRef]
3. Khezri, R.; Mahmoudi, A.; Aki, H. Optimal planning of solar photovoltaic and battery storage systems for grid-connected residential sector: Review, challenges and new perspectives. *Renew. Sustain. Energy Rev.* **2022**, *153*, 111763. [CrossRef]
4. Kant, K.; Biwole, P.H.; Shamseddine, I.; Tlaiji, G.; Pennec, F.; Fardoun, F. Recent advances in thermophysical properties enhancement of phase change materials for thermal energy storage. *Sol. Energy Mater. Sol. Cells* **2021**, *231*, 111309. [CrossRef]
5. Service, R.F. Lithium-ion battery development takes Nobel. *Science* **2019**, *366*, 292. [CrossRef] [PubMed]
6. Endo, M.; Kim, C.; Nishimura, K.; Fujino, T.; Miyashita, K. Recent development of carbon materials for Li ion batteries. *Carbon* **2000**, *38*, 183–197. [CrossRef]
7. Cheng, H.; Shapter, J.G.; Li, Y.; Gao, G. Recent progress of advanced anode materials of lithium-ion batteries. *J. Energy Chem.* **2021**, *57*, 451–468. [CrossRef]
8. Azam, M.A.; Safie, N.E.; Ahmad, A.S.; Yuza, N.A.; Zulkifli, N.S.A. Recent advances of silicon, carbon composites and tin oxide as new anode materials for lithium-ion battery: A comprehensive review. *J. Energy Storage* **2021**, *33*, 102096. [CrossRef]
9. Liu, K.; Liu, Y.; Lin, D.; Pei, A.; Cui, Y. Materials for lithium-ion battery safety. *Sci. Adv.* **2018**, *4*, eaas9820. [CrossRef]
10. Liu, X.-M.; Huang, Z.d.; Oh, S.w.; Zhang, B.; Ma, P.-C.; Yuen, M.M.F.; Kim, J.-K. Carbon nanotube (CNT)-based composites as electrode material for rechargeable Li-ion batteries: A review. *Compos. Sci. Technol.* **2012**, *72*, 121–144. [CrossRef]
11. de las Casas, C.; Li, W. A review of application of carbon nanotubes for lithium ion battery anode material. *J. Power Sources* **2012**, *208*, 74–85. [CrossRef]
12. Zhang, T.; Han, S.; Guo, W.; Hou, F.; Liu, J.; Yan, X.; Chen, S.; Liang, J. Continuous carbon nanotube composite fibers for flexible aqueous lithium-ion batteries. *Sustain. Mater. Technol.* **2019**, *20*, e00096. [CrossRef]
13. Chen, K.; Wang, Q.; Niu, Z.; Chen, J. Graphene-based materials for flexible energy storage devices. *J. Energy Chem.* **2018**, *27*, 12–24. [CrossRef]

14. Dong, Y.; Wu, Z.-S.; Ren, W.; Cheng, H.-M.; Bao, X. Graphene: A promising 2D material for electrochemical energy storage. *Sci. Bull.* **2017**, *62*, 724–740. [CrossRef] [PubMed]

15. Cao, L.; Wang, C.; Huang, Y. Structure optimization of graphene aerogel-based composites and applications in batteries and supercapacitors. *Chem. Eng. J.* **2023**, *454*, 140094. [CrossRef]

16. Wen, Y.; Liu, H.; Jiang, X. Preparation of graphene by exfoliation and its application in lithium-ion batteries. *J. Alloys Compd.* **2023**, *961*, 170885. [CrossRef]

17. Zhang, H.; Yang, Y.; Ren, D.; Wang, L.; He, X. Graphite as anode materials: Fundamental mechanism, recent progress and advances. *Energy Storage Mater.* **2021**, *36*, 147–170. [CrossRef]

18. Natarajan, S.; Divya, M.L.; Aravindan, V. Should we recycle the graphite from spent lithium-ion batteries? The untold story of graphite with the importance of recycling. *J. Energy Chem.* **2022**, *71*, 351–369. [CrossRef]

19. Niu, B.; Xiao, J.; Xu, Z. Advances and challenges in anode graphite recycling from spent lithium-ion batteries. *J. Hazard. Mater.* **2022**, *439*, 129678. [CrossRef]

20. Zhu, X.; Chen, Y.; Xiao, J.; Xu, F.; Su, F.; Yao, Z.; Zhang, Z.; Tang, L.; Zhong, Q. The strategy for comprehensive recovery and utilization of the graphite anode materials from the end-of-life lithium-ion batteries: Urgent status and policies. *J. Energy Storage* **2023**, *68*, 107798. [CrossRef]

21. Yao, N.; Liu, F.; Zou, Y.; Wang, H.; Zhang, M.; Tang, X.; Wang, Z.; Bai, M.; Liu, T.; Zhao, W.; et al. Resuscitation of spent graphite anodes towards layer-stacked, mechanical-flexible, fast-charging electrodes. *Energy Storage Mater.* **2023**, *55*, 417–425. [CrossRef]

22. Sun, L.; Liu, Y.; Shao, R.; Wu, J.; Jiang, R.; Jin, Z. Recent progress and future perspective on practical silicon anode-based lithium ion batteries. *Energy Storage Mater.* **2022**, *46*, 482–502. [CrossRef]

23. Li, Y.; Arnold, S.; Husmann, S.; Presser, V. Recycling and second life of MXene electrodes for lithium-ion batteries and sodium-ion batteries. *J. Energy Storage* **2023**, *60*, 106625. [CrossRef]

24. Wang, Q.; Wu, X.; You, H.; Min, H.; Xu, X.; Hao, J.; Liu, X.; Yang, H. Template-directed Prussian blue nanocubes supported on Ni foam as the binder-free anode of lithium-ion batteries. *Appl. Surf. Sci.* **2022**, *571*, 151194. [CrossRef]

25. Wang, C.-Y.; Liu, T.; Yang, X.-G.; Ge, S.; Stanley, N.V.; Rountree, E.S.; Leng, Y.; McCarthy, B.D. Fast charging of energy-dense lithium-ion batteries. *Nature* **2022**, *611*, 485–490. [CrossRef] [PubMed]

26. Nuhu, B.A.; Bamisile, O.; Adun, H.; Abu, U.O.; Cai, D. Effects of transition metals for silicon-based lithium-ion battery anodes: A comparative study in electrochemical applications. *J. Alloys Compd.* **2023**, *933*, 167737. [CrossRef]

27. Ping, W.; Yang, C.; Bao, Y.; Wang, C.; Xie, H.; Hitz, E.; Cheng, J.; Li, T.; Hu, L. A silicon anode for garnet-based all-solid-state batteries: Interfaces and nanomechanics. *Energy Storage Mater.* **2019**, *21*, 246–252. [CrossRef]

28. Gou, L.; Jing, W.; Li, Y.; Wang, M.; Hu, S.; Wang, H.; He, Y.-B. Lattice-Coupled Si/MXene Confined by Hard Carbon for Fast Sodium-Ion Conduction. *ACS Appl. Energy Mater.* **2021**, *4*, 7268–7277. [CrossRef]

29. Zhu, J.; Gladden, C.; Liu, N.; Cui, Y.; Zhang, X. Nanoporous silicon networks as anodes for lithium ion batteries. *Phys. Chem. Chem. Phys. PCCP* **2013**, *15*, 440–443. [CrossRef]

30. Li, Y.; Yan, K.; Lee, H.-W.; Lu, Z.; Liu, N.; Cui, Y. Growth of conformal graphene cages on micrometre-sized silicon particles as stable battery anodes. *Nat. Energy* **2016**, *1*, 15029. [CrossRef]

31. Song, T.; Jeon, Y.; Samal, M.; Han, H.; Park, H.; Ha, J.; Yi, D.K.; Choi, J.-M.; Chang, H.; Choi, Y.-M.; et al. A Ge inverse opal with porous walls as an anode for lithium ion batteries. *Energy Environ. Sci.* **2012**, *5*, 9028–9033. [CrossRef]

32. Bogart, T.D.; Chockla, A.M.; Korgel, B.A. High capacity lithium ion battery anodes of silicon and germanium. *Curr. Opin. Chem. Eng.* **2013**, *2*, 286–293. [CrossRef]

33. Liang, S.; Cheng, Y.-J.; Zhu, J.; Xia, Y.; Müller-Buschbaum, P. A Chronicle Review of Nonsilicon (Sn, Sb, Ge)-Based Lithium/Sodium-Ion Battery Alloying Anodes. *Small Methods* **2020**, *4*, 2000218. [CrossRef]

34. Fugattini, S.; Gulzar, U.; Andreoli, A.; Carbone, L.; Boschetti, M.; Bernardoni, P.; Gjestila, M.; Mangherini, G.; Camattari, R.; Li, T.; et al. Binder-free nanostructured germanium anode for high resilience lithium-ion battery. *Electrochim. Acta* **2022**, *411*, 139832. [CrossRef]

35. Wu, S.; Wu, H.; Zou, M.; Shi, X.; Yuan, Y.; Bai, W.; Cao, A. Short-range ordered graphitized-carbon nanotubes with large cavity as high-performance lithium-ion battery anodes. *Carbon* **2020**, *158*, 642–650. [CrossRef]

36. Zhu, G.; Tang, C.; Jiang, M.; Du, A.; Zhang, H.; Yang, J. Regulating the interfacial behavior of carbon nanotubes for fast lithium storage. *Electrochim. Acta* **2021**, *388*, 138591. [CrossRef]

37. Qiu, T.-C.; Shao, Z.-G.; Wang, C.-L.; Yang, L. QPHT graphene as a high-performance lithium ion battery anode materials with low diffusion barrier and high capacity. *Phys. Lett. A* **2022**, *456*, 128549. [CrossRef]

38. Wang, B.; Ruan, T.; Chen, Y.; Jin, F.; Peng, L.; Zhou, Y.; Wang, D.; Dou, S. Graphene-based composites for electrochemical energy storage. *Energy Storage Mater.* **2020**, *24*, 22–51. [CrossRef]

39. Du, J.; Zhang, Y.; Deng, S.; Xu, N.; Xiao, Z.; She, J.; Wu, Z.; Cheng, H. Correlation between topographic structures and local field emission characteristics of graphene-sheet films. *Carbon* **2013**, *61*, 507–514. [CrossRef]

40. Fan, Z.; Yan, J.; Ning, G.; Wei, T.; Zhi, L.; Wei, F. Porous graphene networks as high performance anode materials for lithium ion batteries. *Carbon* **2013**, *60*, 558–561. [CrossRef]

41. Zeferino González, I.; Chiu, H.-C.; Gauvin, R.; Demopoulos, G.P.; Miki-Yoshida, M.; Valenzuela-Muñiz, A.M.; Verde-Gómez, Y. Graphene nanobuds as a novel anode design paradigm with superior Li-ion storage capacity and rate capability. *Carbon* **2022**, *199*, 486–496. [CrossRef]

42. Meng, C.; Yuan, M.; Cao, B.; Lin, X.; Zhang, J.; Li, A.; Chen, X.; Jia, M.; Song, H. Laser-modified graphitic onion-like carbon as anode for lithium/potassium-ion batteries. *Carbon* **2022**, *192*, 347–355. [CrossRef]
43. Khosla, N.; Narayan, J.; Narayan, R.; Sun, X.-G.; Paranthaman, M.P. Microstructure and defect engineering of graphite anodes by pulsed laser annealing for enhanced performance of lithium-ion batteries. *Carbon* **2023**, *205*, 214–225. [CrossRef]
44. Zhou, Y.-Q.; Dong, X.-L.; Li, W.-C.; Hao, G.-P.; Yan, D.; Lu, A.-H. Millimeter-sized few-layer graphene sheets with aligned channels for fast lithium-ion charging kinetics. *J. Energy Chem.* **2021**, *55*, 62–69. [CrossRef]
45. Li, R.; Huang, J.; Ren, J.; Cao, L.; Li, J.; Li, W.; Lu, G.; Yu, A. A sandwich-like porous hard carbon/graphene hybrid derived from rapeseed shuck for high-performance lithium-ion batteries. *J. Alloys Compd.* **2020**, *818*, 152849. [CrossRef]
46. Ning, G.; Xu, C.; Cao, Y.; Zhu, X.; Jiang, Z.; Fan, Z.; Qian, W.; Wei, F.; Gao, J. Chemical vapor deposition derived flexible graphene paper and its application as high performance anodes for lithium rechargeable batteries. *J. Mater. Chem. A* **2013**, *1*, 408. [CrossRef]
47. Chen, S.; Bao, P.; Xiao, L.; Wang, G. Large-scale and low cost synthesis of graphene as high capacity anode materials for lithium-ion batteries. *Carbon* **2013**, *64*, 158–169. [CrossRef]
48. Liu, C.; Xiao, N.; Wang, Y.; Li, H.; Wang, G.; Dong, Q.; Bai, J.; Xiao, J.; Qiu, J. Carbon clusters decorated hard carbon nanofibers as high-rate anode material for lithium-ion batteries. *Fuel Process. Technol.* **2018**, *180*, 173–179. [CrossRef]
49. Ma, C.; Zhao, Y.; Li, J.; Song, Y.; Shi, J.; Guo, Q.; Liu, L. Synthesis and electrochemical properties of artificial graphite as an anode for high-performance lithium-ion batteries. *Carbon* **2013**, *64*, 553–556. [CrossRef]
50. Ma, C.; Zhao, Y.; Li, J.; Song, Y.; Shi, J.; Guo, Q.; Liu, L. The electrochemical performance of pitch coke anodes containing hollow carbon nanostructures and nickel nanoparticles for high-power lithium ion batteries. *Electrochim. Acta* **2013**, *112*, 394–402. [CrossRef]
51. Li, L.; Zhang, D.; Deng, J.; Gou, Y.; Fang, J.; Cui, H.; Zhao, Y.; Cao, M. Carbon-based materials for fast charging lithium-ion batteries. *Carbon* **2021**, *183*, 721–734. [CrossRef]